Supporting Information

Selective improvement of NO$_2$ gas sensing behavior in SnO$_2$ nanowires by ion-beam irradiation

Yong Jung Kwon[1], Sung Yong Kang[1], Ping Wu [2,*], Yuan Peng[2], Sang Sub Kim[3,*], Hyoun Woo Kim[1,*]

[1]Division of Materials Science and Engineering, Hanyang University, Seoul 133-791, Republic of Korea

[2]Entropic Interface Group, Singapore University of Technology & Design, Singapore 138682, Singapore

[3]Department of Materials Science and Engineering, Inha University, Incheon 402-751, Republic of Korea

[*]Corresponding authors: hyounwoo@hanyang.ac.kr; sangsub@inha.ac.kr; wuping@sutd.edu.sg

Text S1.

According to the SRIM calculation, all He ions under the ion beam condition used in this study penetrate through the SnO_2 nanowire because the average projected range of He ions in SnO_2 at the accelerating voltage of 45 MeV is calculated to be ~400 μm, which is far larger than the diameter of the SnO_2 nanowires. Accordingly, almost no energy loss of the He ions will be expected. That is, the energy of the ions throughout the trajectory is continuously about 45 MeV. In this case, one He ion deposits the energies of 66.78 keV/micron (6.678 eV/Angstrom) and 0.0335 keV/micron (0.00335eV/Angstrom), by electronic stopping and nuclear stopping, respectively. In this case, the electronic stopping is dominant, with the nuclear stopping being negligible. The average atomic density of SnO_2 is about 10 atoms/nm (or 1 atom/Angstrom). So, 1 atom (O or Sn) on the He ion trajectory gets about 6.678 eV from one He ion of 45 MeV by the electronic stopping. We think that the formation energies of O vacancies or Sn interstitials in the SnO_2 lattice are intrinsic. Formation energies of intrinsic defects will be dependent on a variety of factors, including the Fermi energy. For example, under O-poor and H-rich conditions, the formation energy of Sn interstitials (Sn_i) ranges from about -3 to +6 eV, with varying the Fermi energy in the range of 0-3 eV.[1] Also, the formation energy of oxygen vacancies (V_O) ranges from about -1 to +2 eV, with varying the Fermi energy in the range of 0-3 eV.[1] Accordingly, with the calculation that O or Sn atoms will get about 6.678 eV from one He ion, there is a chance that the trajectory energy enforced by one He ion is greater than the formation energy of tin interstitials and/or oxygen vacancies.
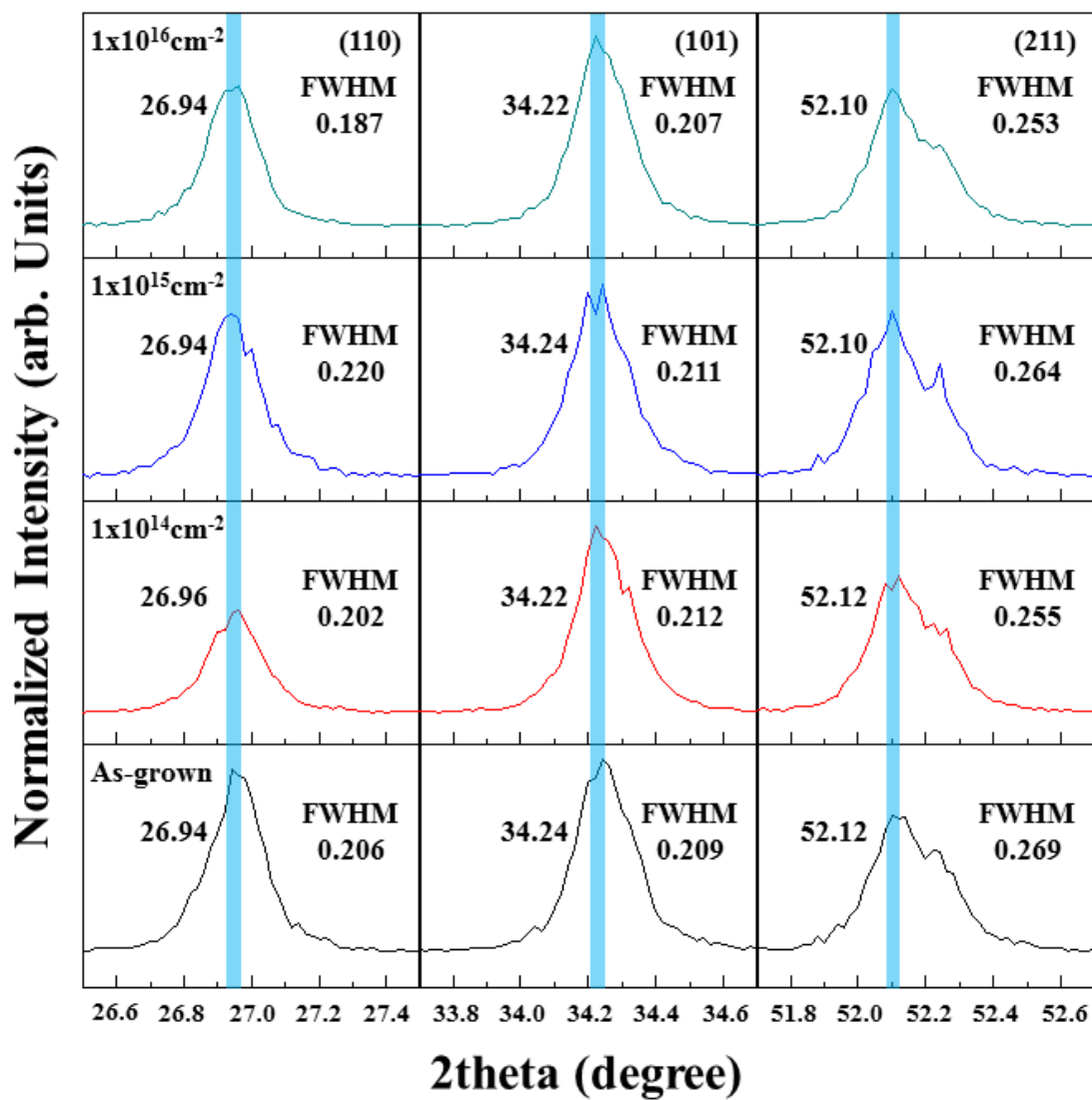
Figure S1. Peak positions and FWHM values of the main XRD peaks, including (110), (101), and (211).
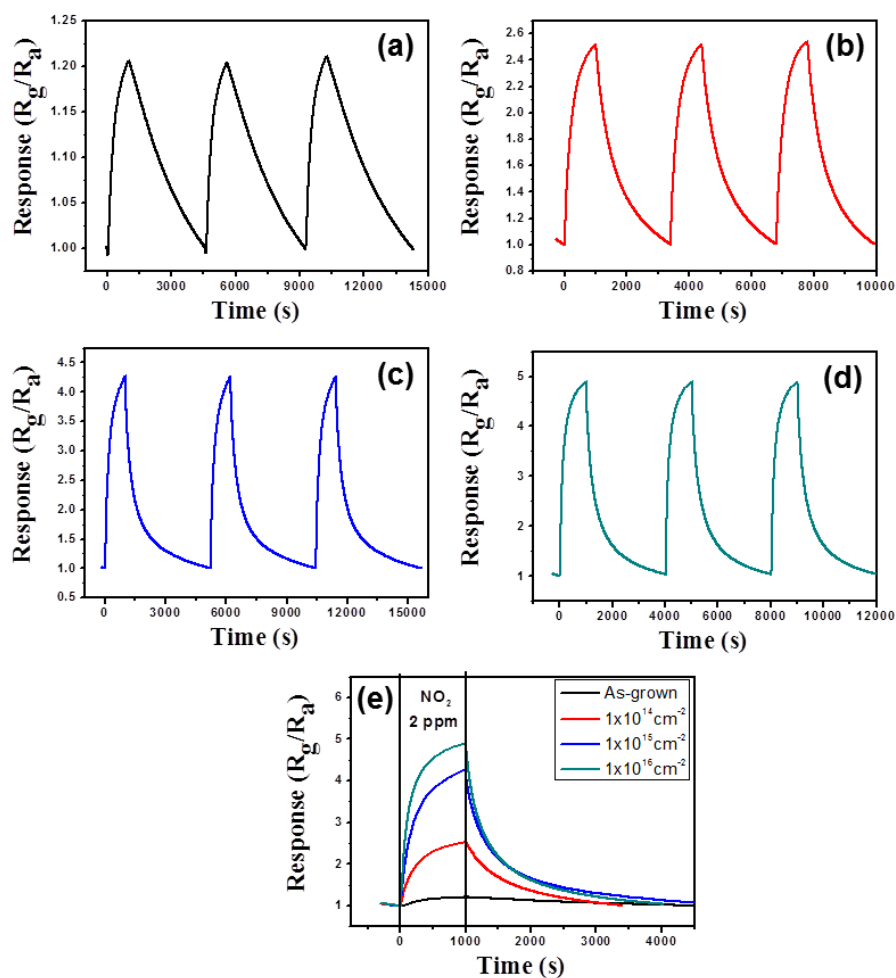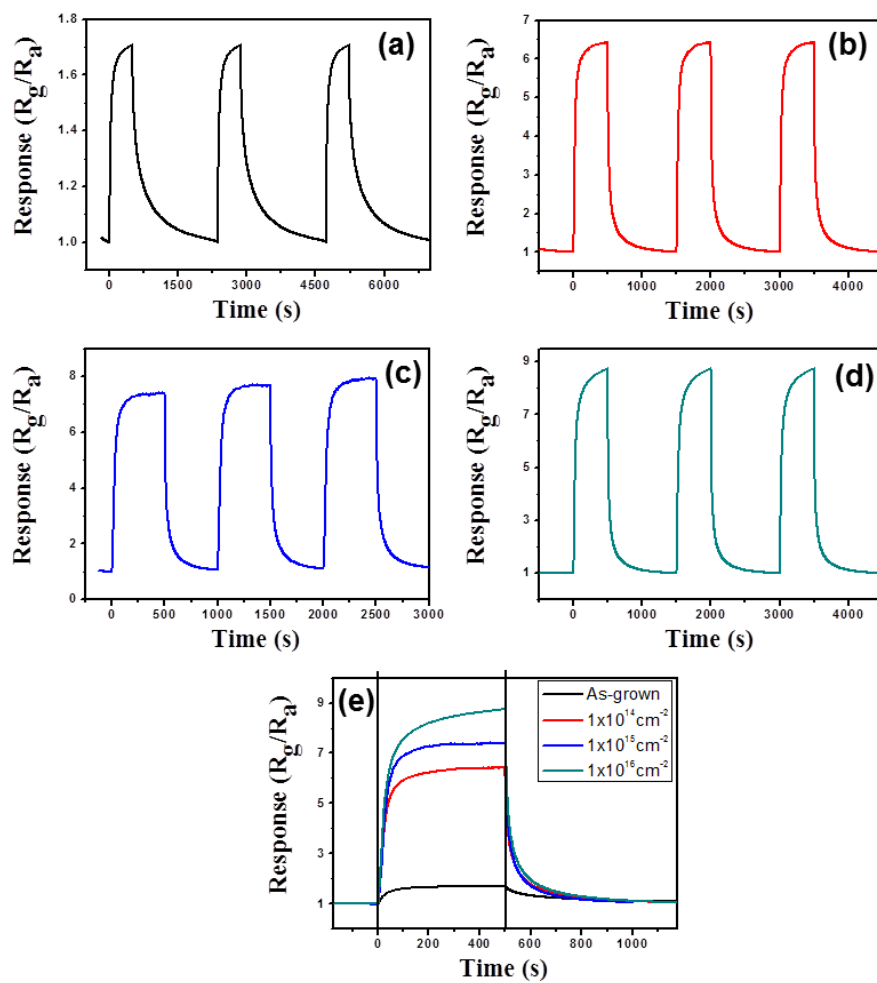
Figure S2. Sensor responses of SnO_2 nanowires, (a) which were unirradiated, (b-d)) irradiated at a fluence of (b) $1x10^{14}$, (c) $1x10^{15}$, and (d) $1x10^{16}$ ions/cm^2. (e) Summary of sensor response curves for 4 samples. The sensing temperature and the NO_2 concentration were set to 25°C and 2 ppm, respectively.
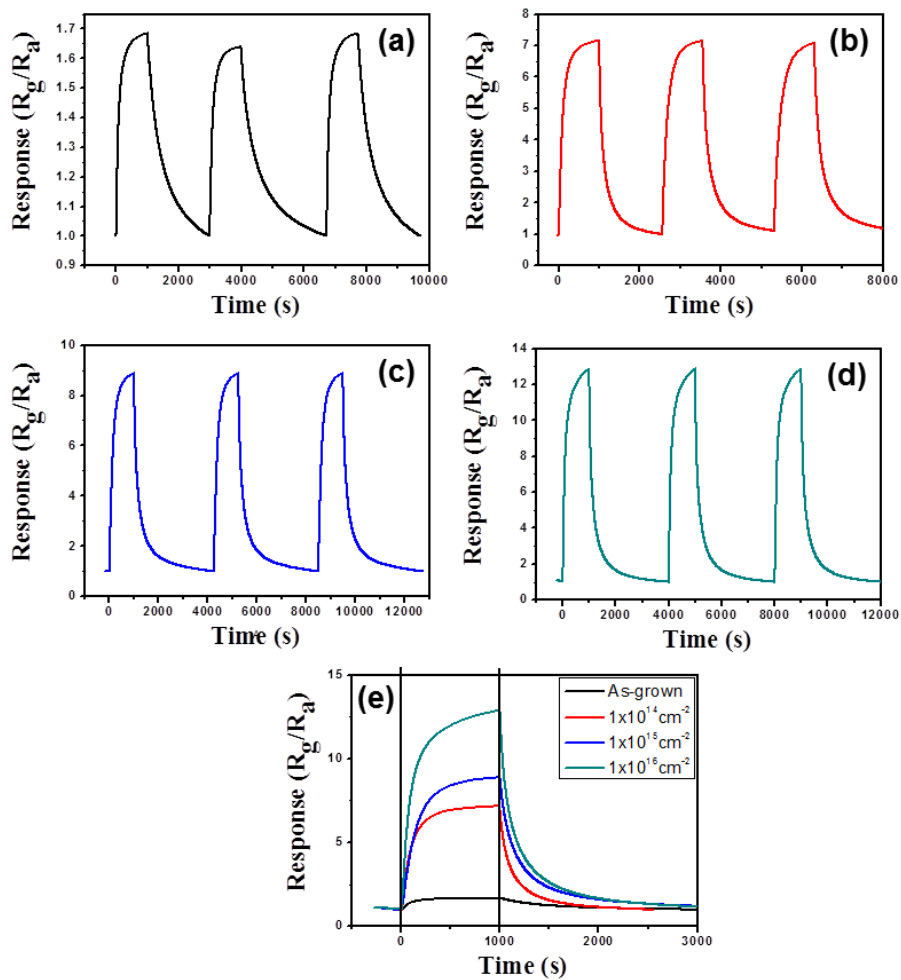
Figure S3. Sensor responses of SnO_2 nanowires, (a) which were unirradiated, (b-d)) irradiated at a fluence of (b) $1x10^{14}$, (c) $1x10^{15}$, and (d) $1x10^{16}$ ions/cm^2. (e) Summary of sensor response curves for 4 samples. The sensing temperature and the NO_2 concentration were set to 100°C and 2 ppm, respectively.
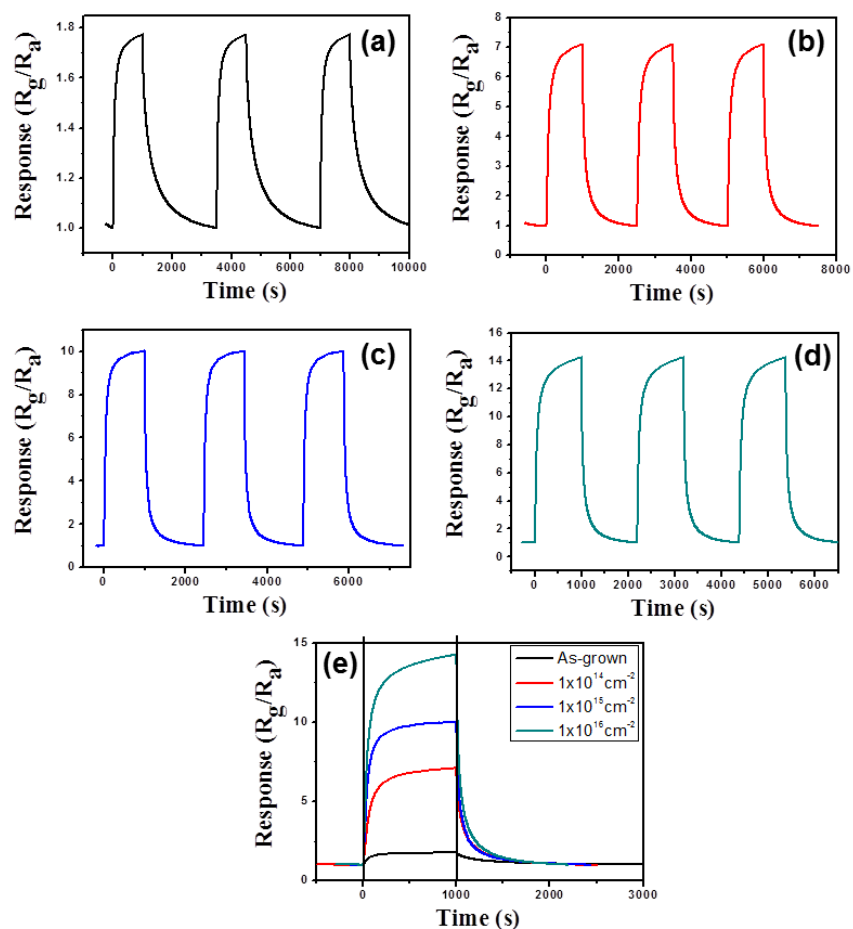
Figure S4. Sensor responses of SnO$_2$ nanowires, (a) which were unirradiated, (b-d)) irradiated at a fluence of (b) 1x10^{14}, (c) 1x10^{15}, and (d) 1x10^{16} ions/cm^2. (e) Summary of sensor response curves for 4 samples. The sensing temperature and the NO$_2$ concentration were set to 150°C and 2 ppm, respectively.
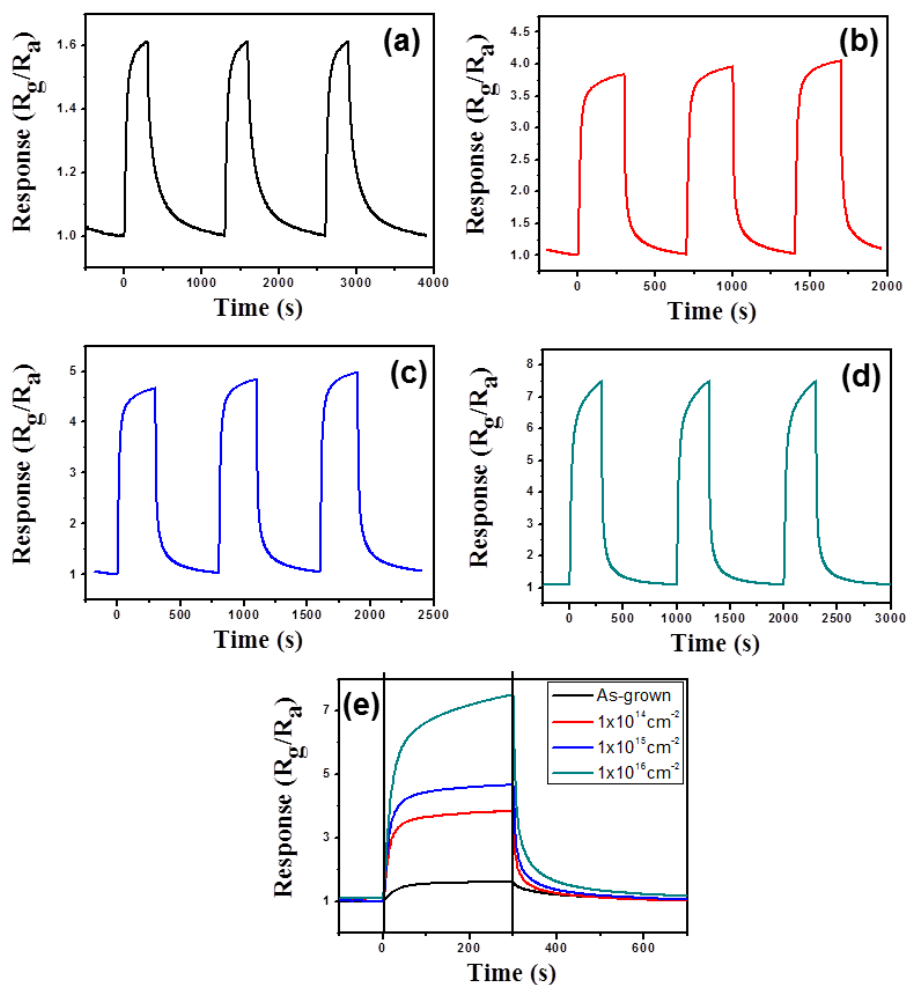
Figure S5. Sensor responses of SnO_2 nanowires, (a) which were unirradiated, (b-d)) irradiated at a fluence of (b) 1×10^{14}, (c) 1×10^{15}, and (d) 1×10^{16} ions/cm^2. (e) Summary of sensor response curves for 4 samples. The sensing temperature and the NO_2 concentration were set to 200°C and 2 ppm, respectively.

Figure S6. Sensor responses of SnO_2 nanowires, (a) which were unirradiated, (b-d)) irradiated at a fluence of (b) $1x10^{14}$, (c) $1x10^{15}$, and (d) $1x10^{16}$ ions/cm^2. (e) Summary of sensor response curves for 4 samples. The sensing temperature and the NO_2 concentration were set to 250°C and 2 ppm, respectively.
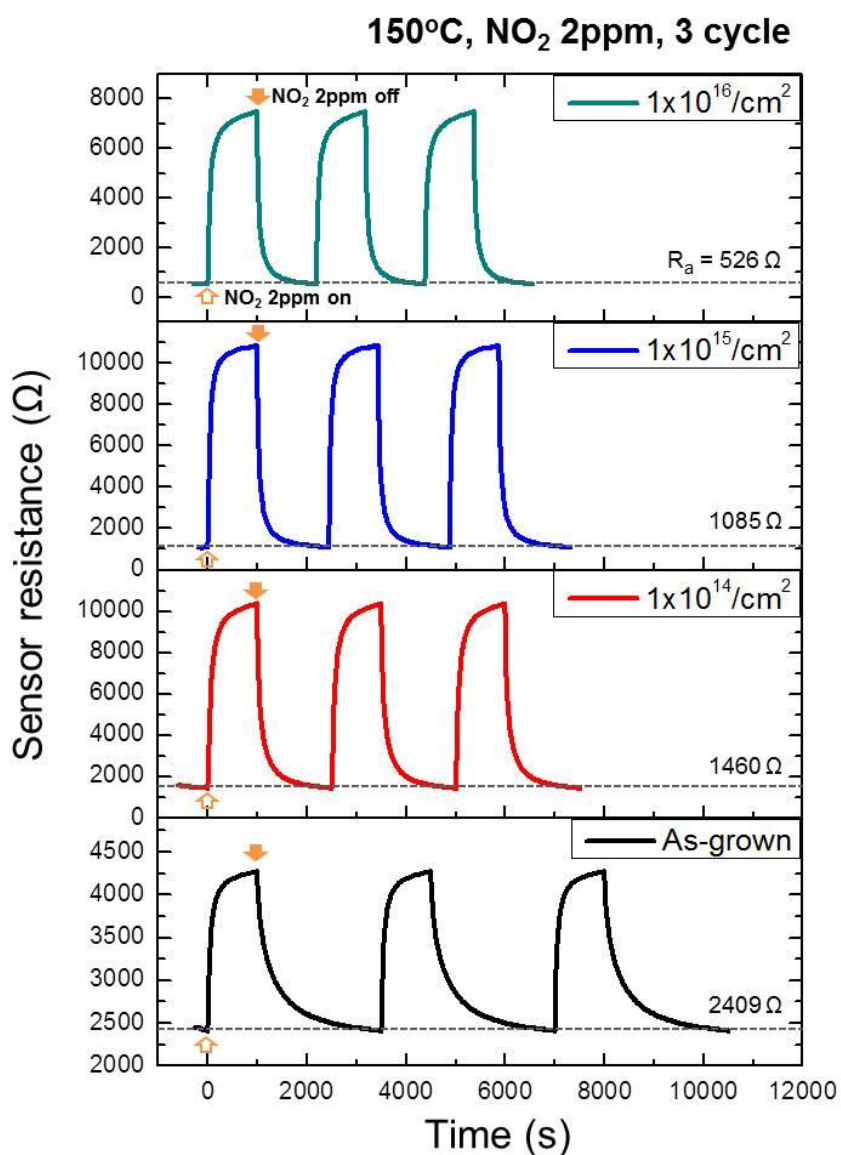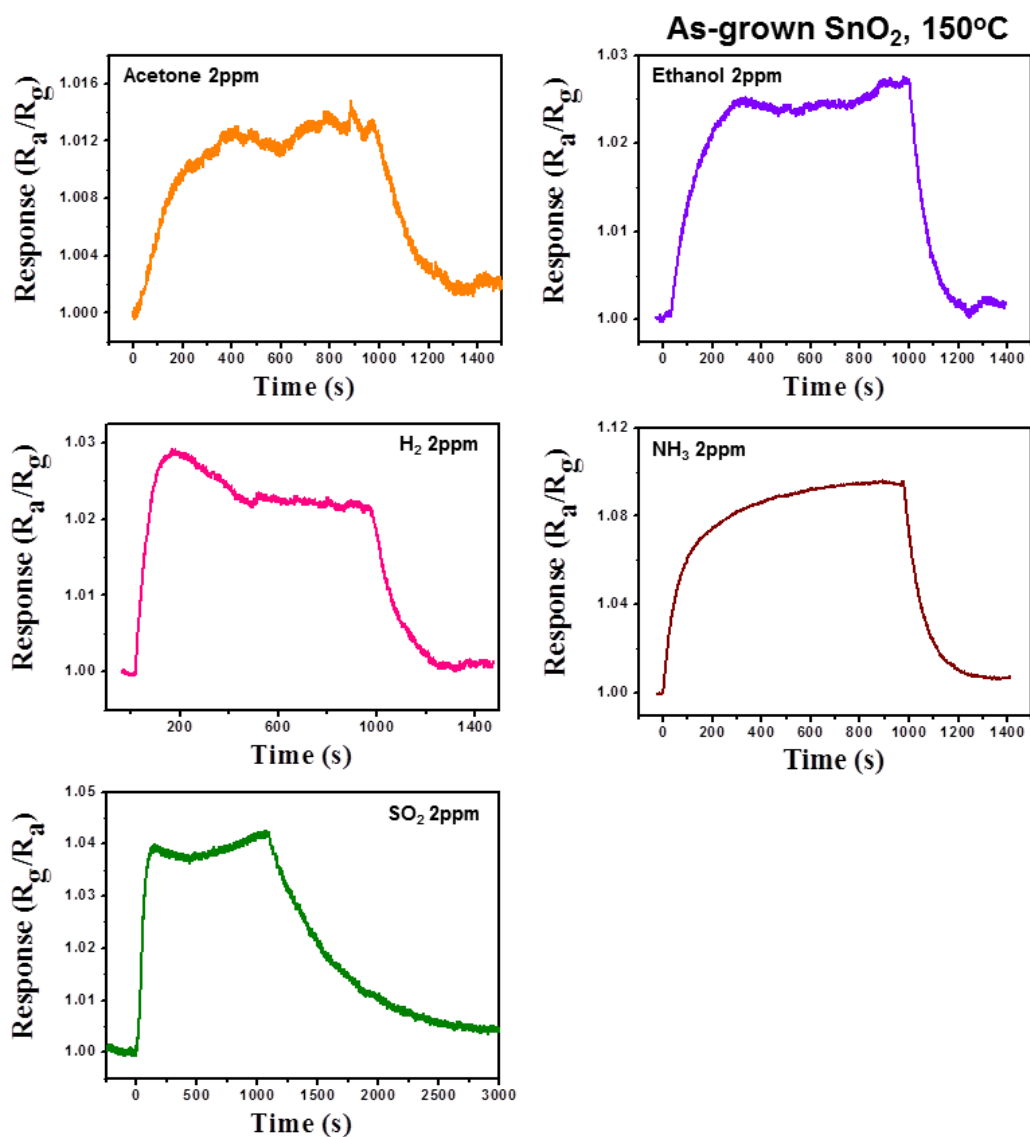
150°C, NO₂ 2ppm, 3 cycle

Figure S7. Dynamic resistance curves for three cycles at NO₂ concentration and temperature of 2 ppm and 150°C, respectively, for the sensors fabricated from the samples, which were unirradiated and irradiated SnO₂ nanowires. The ion fluences were set to 1×10^{14}, 1×10^{15}, and 1×10^{16} ions/cm², respectively.

Figure S8. Dynamic response curves of SnO_2 nanowires to acetone, ethanol, H_2, NH_3, and SO_2 gases, which were unirradiated. The sensing temperature and the gas concentration were set to $150°C$ and 2 ppm, respectively.
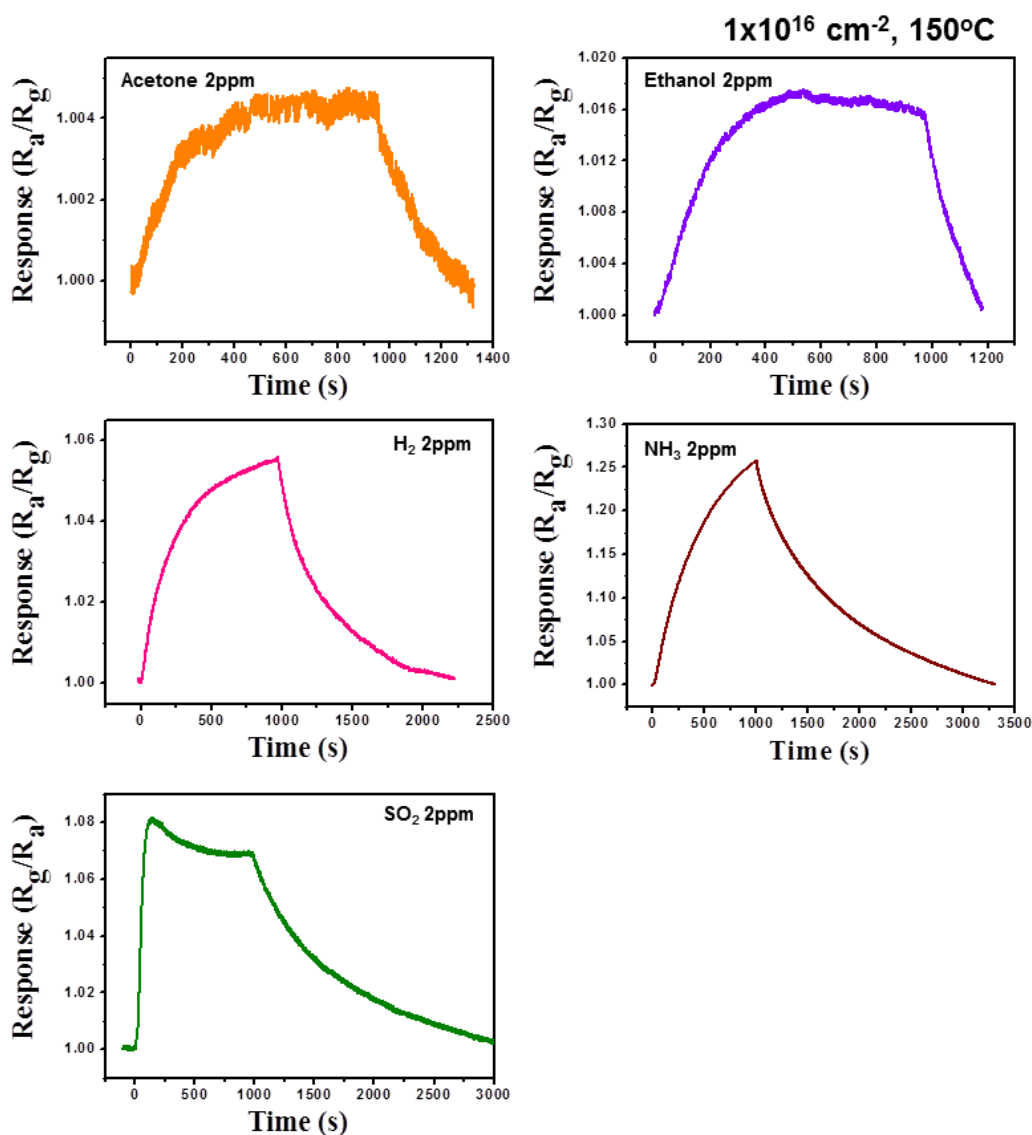
Figure S9. Dynamic response curves of SnO$_2$ nanowires to acetone, ethanol, H$_2$, and NH$_3$, and SO$_2$ gases, which were irradiated at a fluence of 1x10^{16} ions/cm^2. The sensing temperature and the gas concentration were set to 150°C and 2 ppm, respectively.
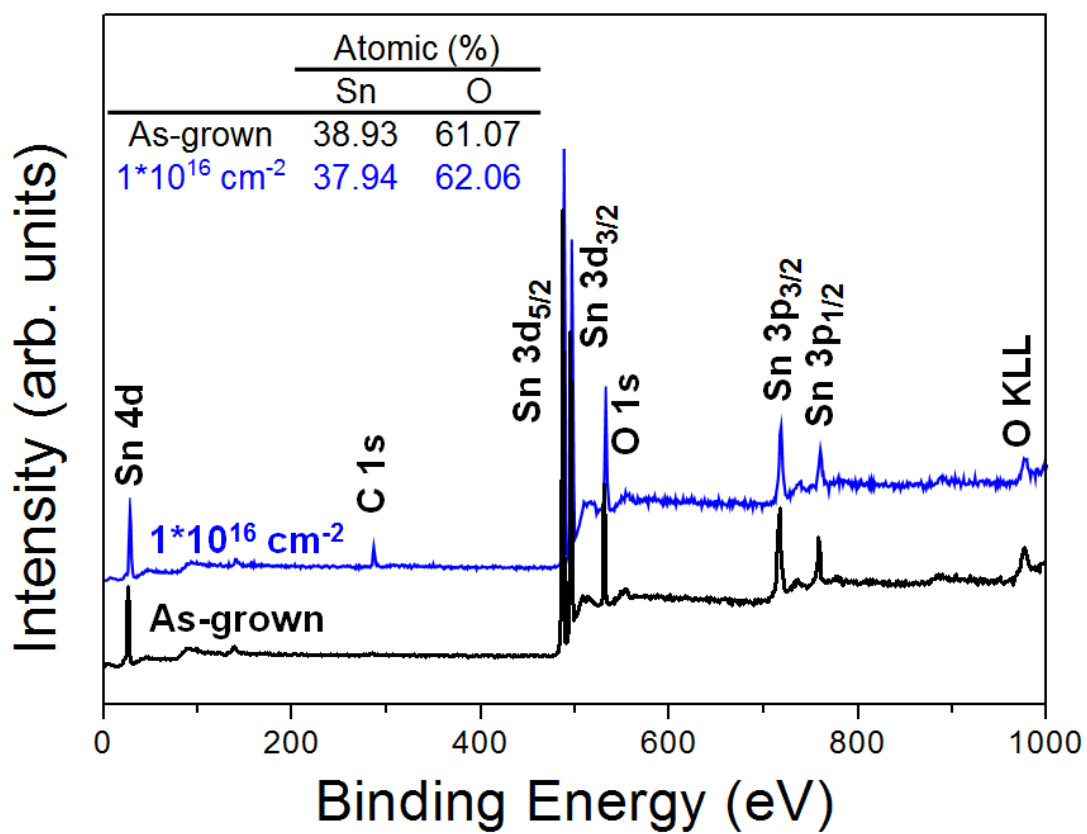
Figure S10. XPS survey spectra of unirradiated and irradiated SnO_2 nanowires. The ion fluences were set to $1x10^{16}$ ions/cm^2.
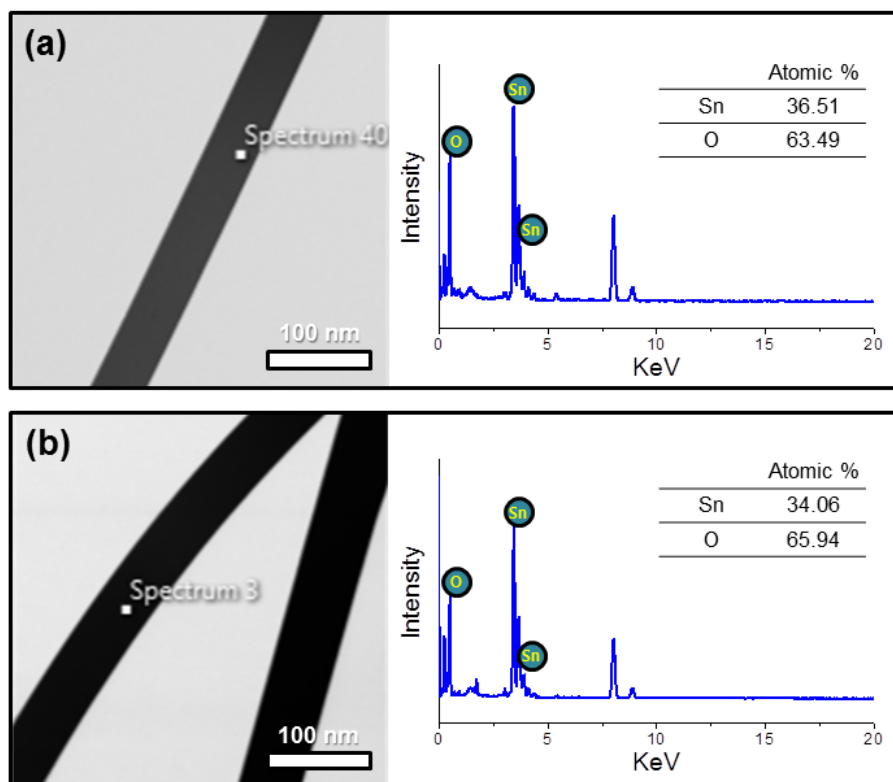
Figure S11. Typical TEM image and corresponding EDS patterns of (a) unirradiated and (b) irradiated SnO_2 nanowires. The ion fluence was set to 1×10^{16} ions/cm^2.

Table S1. Summary of the sensor responses of various samples to NO_2 gas at a concentration of 2 ppm.

	NO$_2$ 2ppm gas response (R$_g$/R$_a$)				
	RT	100°C	150°C	200°C	250°C
As-grown	1.2	1.7	1.8	1.7	1.6
1×10^{14} ions/cm^2	2.5	7.2	7.1	6.4	3.8
1×10^{15} ions/cm^2	4.3	8.9	10.0	7.4	4.7
1×10^{16} ions/cm^2	4.9	12.9	14.2	8.7	7.5

Table S2. Summary of the sensor responses of SnO_2 nanowires without and with the ion beam irradiation, to NO_2, SO_2, NH_3, H_2, acetone, and ethanol gases. The concentration was set to 2 ppm.

	Gas response (R_a/R_g or R_g/R_a)					
	NO_2	SO_2	NH_3	H_2	Acetone	Ethanol
As-grown	1.8	1.0	1.1	1.0	1.0	1.0
$1\times10^{16}\ cm^{-2}$	14.2	1.1	1.3	1.1	1.0	1.0

Table S3. Gas sensing abilities of the gas sensors activated by the beam-irradiation.

Nanostructure type	Beam species	Sensing gases	Max. Response (R_a/R_g or R_g/R_a) (at temp./conc.)	Increase in sensitivity		Reference
Cu$_x$S thin films	Au heavy ions [100 MeV]	NH$_3$	1.28	3.2%	-	2
Ag/Ag$_2$SnO$_3$ nanoparticles	Gamma ray [400 kGy]	Acetic acid	~2 (400 ppm)	10.6 fold	-	3
ZnO nanorods	UV	O$_2$	~5.2 (50℃)	4.66 fold		4
Polycrystalline SnO$_2$ [simulation]	UV	Reducing gas	~20 (grain size = 10 nm)	9 fold		5
Undoped SnO$_2$ thin films	Ni$^+$ ions [75 MeV]	NH$_3$	4.2 [250℃/1000ppm]	~133%		6
SnO$_2$ thin films	UV	LPG	64.9 (25℃/200 ppm)	~64 fold	Even >2400-fold increase in SnO$_2$-Pt structures	7
In$_2$Te$_3$ thin films	Au ion [130 MeV]	CO$_2$	~1.5 (1000 ppm)	-		8
ZnO film	Visible light	Ethylene Aceton	1.05 [25℃/5200 ppm] 1.20 [25℃/900 ppm]	5% 20%		9
Reduced graphene oxide	Electron beam	NO$_2$	~1.01 (25℃/10 ppm)	~ 1%	Response time ~83% decreased	10
Au-sputtered TiO$_2$ nanofibers	UV	H$_2$	~95 [190℃/200 ppm]	~15 fold	Response [recovery] time ~70 [83] % decreased	11
Carbon nanotube films	Laser [Nd:YAG]	NO	~1.034 [150℃/200 ppm]	~1%		12
SnO$_2$-reduced graphite oxide monolayer-ordered porous films	UV	ethanol	~108 [175℃/400 ppm]	~36 fold	-	13
SnO$_2$ nanowires	**He ion beam**	**NO$_2$**	**14.24 (150℃/ 2ppm)**	**~ 7 fold**		**Present work**

REFERENCES

(1) Kilic, C.; Zunger, A. Origins of Coexistence of Conductivity and Transparency in SnO_2. *Phys. Rev. Lett.* **2002**, 88, 095501.

(2) Sagade, A. A.; Sharma, R.; Sulaniya, I. Enhancement in Sensitivity of Copper Sulfide Thin Film Ammonia Gas Sensor: Effect of Swift Heavy Ion Irradiation. *J. Appl. Phys.* **2009**, 105, 043701.

(3) Yin, K.; Liao, F.; Zhu, Y.; Gao, A.; Wang, T.; Shao, M. Enhanced Gas-Sensing Response by Gamma Ray Irradiation: Ag/Ag_2SnO_3 Nanoparticle-Based Sensor to Ethanol, Nitromethane and Acetic Acid. *J. Mater. Chem. C* **2014**, 2, 10082-10086.

(4) Chou, C.-S.; Wu, Y.-C.; Lin, C.-H. Oxygen Sensor Utilizing Ultraviolet Irradiation Assisted ZnO Nanorods under Low Operation Temperature. *RSC Adv.* **2014**, 4, 52903-52910.

(5) Mishra, S.; Ghanshyam, C.; Ram, N.; Bajpai, R. P.; Bedi, R. K. Detection Mechanism of Metal Oxide Gas Sensor under UV Radiation. *Sens. Actuators B* **2004**, 97, 387-390.

(6) Rani, S.; Bhatnagar, M. C.; Roy, S. C.; Puri, N. K.; Kanjilal, D. P-Type Gas-Sensing Behavior of Undoped SnO_2 Thin Films Irradiated with A High-Energy Ion Beam. *Sens. Actuators B* **2008**, 135, 35-39.

(7) Haridas, D.; Chowdhuri, A.; Sreenivas, K.; Gupta, V. Enhanced Room Temperature Response of SnO_2 Thin Film Sensor Loaded with Pt Catalyst Clusters under UV Radiation for LPG. *Sens. Actuators B* **2011**, 135 152-157.

(8) Matheswaran, P.; Sathyamoorthy, R.; Asokan, K. Effect of 130 Mev Au Ion Irradiation on CO_2 Gas Sensing Properties of In_2Te_3 Thin Films. *Sens. Actuators B* **2013**, 177, 8-13.

(9) Geng, Q.; He, Z.; Chen, X.; Dai, W.; Wang, X. Gas Sensing Property of ZnO under Visible Light Irradiation at Room Temperature. *Sens. Actuators B* **2013**, 188, 293-297.

(10) Kwon, Y. J.; Cho, H. Y.; Na, H. G.; Lee, B. C.; Kim, S. S.; Kim, H. W. Improvement of Gas Sensing Behavior in Reduced Graphene Oxides by Electron-beam Irradiation. *Sens. Actuators B* **2014**, 203, 143-149.

(11) Nikfarjam, A.; Salehifar, N. Improvement in Gas-Sensing Properties of TiO_2 Nanofiber Sensor by UV Irradiation. *Sens. Actuators B* **2015**, 211, 146-156.

(12) Ueda, T.; Katsuki, S.; Abhari, N. H.; Ikegami, T.; Mitsugi, F.; Nakamiya, T. Effect of Laser Irradiation on Carbon Nanotube Films for NO_x Gas Sensor. *Surf. Coat. Technol.* **2008**, 202, 5325-5328.

(13) Xu, S.; Sun, F.; Yang, S.; Pan, Z.; Long, J.; Gu, F. Fabrication of SnO_2-Reduced Graphite Oxide Monolayer-Ordered Porous Film Gas Sensor with Tunable Sensitivity through Ultra-Violet Light Irradiation. *Sci. Rep.* 2015, DOI: 10.1038/srep08939.